Open access • Posted Content • DOI:10.1101/2020.05.21.109397

BRAFV600E induces reversible mitotic arrest in human melanocytes via microRNA-mediated suppression of AURKB — Source link

Andrew S. McNeal, Rachel L. Belote, Hanlin Zeng, Marcus Urquijo ...+19 more authors

Institutions: University of California, San Francisco, Huntsman Cancer Institute, University of Utah, San Francisco VA Medical Center

Published on: 20 May 2021 - bioRxiv (Cold Spring Harbor Laboratory)

Topics: Nevus, Nevi and melanomas and Melanocytic nevus

MicroRNAs Restrain Proliferation in BRAF^{V600E} Melanocytic Nevi

Authors and Affiliations:

Andrew S. McNeal
Helen Diller Family Comprehensive Cancer Center, University of California San Francisco

Rachel L. Belote*
Huntsman Cancer Institute, University of Utah

Hanlin Zeng*
Huntsman Cancer Institute, University of Utah

Kendra Barker
Huntsman Cancer Institute, University of Utah

Rodrigo Torres
Helen Diller Family Comprehensive Cancer Center, Department of Dermatology, University of California San Francisco

A. Hunter Shain
Helen Diller Family Comprehensive Cancer Center, Department of Dermatology, University of California San Francisco

Robert H. I. Andtbacka
Huntsman Cancer Institute, Department of Surgery, University of Utah

Sheri L. Holmen
Huntsman Cancer Institute, Department of Surgery, University of Utah

David H. Lum
Huntsman Cancer Institute, University of Utah

Timothy H. McCalmont
Department of Pathology, Department of Dermatology, University of California San Francisco

Matthew W. VanBrocklin
Huntsman Cancer Institute, Department of Surgery, University of Utah

Maria L. Wei
Helen Diller Family Comprehensive Cancer Center, Department of Dermatology, University of California San Francisco, San Francisco Veterans Affairs Medical Center

Ursula E. Lang
Helen Diller Family Comprehensive Cancer Center, Department of Pathology, Department of Dermatology, University of California San Francisco

Robert L. Judson-Torres
Helen Diller Family Comprehensive Cancer Center, University of California San Francisco, Huntsman Cancer Institute, Department of Dermatology, University of Utah

* Equal contribution

Running Title: microRNAs drive nevus arrest

Keywords: Nevus, Melanoma, microRNA, Skin

Additional Information:
Financial Support: NIH Director's Common Fund – DP5 OD019787 (RLJ), NCI 5F31CA236377 (ASM), and NIC P30CA042014 (University of Utah)

Corresponding Author: Robert L. Judson-Torres 2000 Circle of Hope Drive Salt Lake City, Utah 84112 Phone: (801) 213-8436 Email: judsontorreslab@gmail.com

Abstract:

Benign melanocytic nevi commonly form when melanocytes that acquire a *BRAF*^{V600E} mutation undergo a period of rapid proliferation and subsequent arrest. Constitutive activation of MAPK signaling downstream of BRAF drives the initial proliferative phenotype. However, the factors that establish and maintain growth arrest in nevi remain elusive. The growth-arrested state of *BRAF*^{V600E} melanocytes is not conferred by additional genetic mutations, suggesting a role for regulatory elements. We investigated the role of microRNAs in the initiation and maintenance of nevus arrest. Using primary human melanocytes, melanocytic nevi, and adjacent melanoma, we show that MIR211-5p and MIR328-3p are enriched in nevi compared to normal melanocytes, then subsequently downregulated in adjacent melanoma. Both MIR211-5p and MIR328-3p proved necessary effectors of BRAF^{V600E}-induced growth arrest in human melanocytes. We identified microRNA target networks which, when suppressed, phenocopy BRAF^{V600E}-induced arrest and converge on inhibition of AURKB to block cell cycle progression in primary human melanocytes.

Statement of Significance:

We describe a microRNA regulatory network that enforces BRAF^{V600E}-induced growth arrest in human melanocytes during melanocytic nevus formation. De-regulation of MIR211-5p and MIR328-3p targets – which converge on AURKB – leads to cell cycle re-entry and melanoma progression. AURKB inhibition therefore provides a potential therapeutic intervention for melanoma prevention or treatment.

Introduction:

Cutaneous melanoma is a potentially fatal skin cancer arising from the pigment-producing melanocytes of the basal layer of the human epidermis (1). Despite the development of targeted therapies, such as small molecule inhibitors and immunotherapy, mortality rates of advanced melanoma remain stubbornly high (2). If detected in its earliest stages, however, melanoma can often be cured through surgical excision (3) (4).

Acquired activating V600E mutations in the BRAF proto-oncogene drive approximately 50% of all cutaneous melanomas (5) (6). Yet, when a melanocyte acquires a $BRAF^{V600E}$ mutation alone, the cell does not immediately transform to cancer. Instead, it undergoes rapid clonal proliferation followed by growth arrest resulting in a stable pigmented skin macule known as a benign nevus or mole (7) (8). Despite the continued expression of $BRAF^{V600E}$, the majority of nevi remain innocuous for the lifespan of the individual, suggesting that nevus cells have robust intrinsic defenses against hyperproliferation.

Aberrant MAP kinase signaling downstream of $BRAF^{V600E}$ produces a cascade of intracellular changes, each of which may contribute to the establishment and/or maintenance of growth arrest. $BRAF^{V600E}$ expression has been shown to induce negative feed-back loops that ultimately dampen MAP kinase signaling (9). DNA hyper-replication from oncogenic activation can simultaneously deplete cellular nucleotide pools and trigger DNA damage response pathways (10) (11). In addition, epigenetic remodeling of chromatin has been observed in nevi, suggesting that transcriptional reprogramming contributes to growth arrest (12). For example, increased gene expression of cyclin dependent kinase 4/6 (CDK4/6) inhibitors, such as $p16^{INK4A}$ and $p15^{INK4B}$, is associated with benign nevi (13) (14) (15).

Although each of these factors likely contributes to the growth arrest phenotype of stable melanocytic nevi, the mechanisms that drive the bi-phasic process of nevogenesis – temporary proliferation prior to growth arrest - remain elusive. DNA sequencing of human nevi revealed that growth-arrested $BRAF^{V600E}$ melanocytes have no additional genetic changes that would

distinguish them from their proliferative precursors (16), suggesting that transcriptional regulation is crucial for establishing the bi-phasic phenotype and ultimately restraining hyperproliferation. Interestingly, the growth restraint itself is non-permanent. Outside the context of transformation, nevus melanocytes can also re-enter the cell cycle following exposure to specific stimuli, as seen in cases of recurrent nevi (17) or widespread nevus eruption (18). Further, it remains unclear how the known mechanisms governing nevus growth arrest are overcome during melanoma initiation. For example, while $p16^{INK4A}$ is expressed in the majority of nevi, >80% of melanoma *in situ* outgrowths from nevi and 40% of advanced melanomas retain its expression (15) (19) (20) (21) (22) (23). Furthermore, knockdown or deletion of $p16^{INK4A}$ fails to overcome $BRAF^{V600E}$-induced arrest (13) (15). Insight into the mechanisms that distinguish $BRAF^{V600E}$-driven melanocyte expansion, growth arrest, and escape could reveal new approaches for detection, prevention, and therapeutic intervention in melanoma.

A unifying characteristic of $BRAF^{V600E}$-induced growth arrest pathways is the remodeling of the melanocyte transcriptome, which must remain durable to prevent nevus transformation to melanoma. MicroRNAs are small non-coding RNAs that regulate networks of genes and confer robustness to transcriptional programs (24). Aberrant microRNA expression has been reported in numerous human cancers, including melanoma, where they have been shown to play both oncogenic and tumor suppressive roles (25) (26) (27) (28). MicroRNAs regulate biological processes through complementary binding to the 3' untranslated region (3' UTR) of mRNA networks, and therefore can serve as useful probes for unraveling complex transcriptional programs (29) (30) (31) (32). Seminal studies of gene networks targeted by miRNAs specific to aggressive melanoma revealed mechanisms required for metastatic dissemination (31). Here, we have taken a similar approach to unravel the mechanisms driving nevogenesis and melanoma initiation. Using clinical specimens of conventional human nevi with adjacent melanoma, and primary human melanocytes derived from both normal skin and nevi, we identified elevated MIR211-5p and MIR328-3p expression as part of a nevus-specific

transcriptome. Expression of both microRNAs mediates $BRAF^{V600E}$ - induced growth arrest by regulating networks of dozens of genes. Both microRNAs converge to inhibit aurora kinase B (AURKB) translation, which is required to induce growth arrest in $BRAF^{V600E}$ melanocytes and melanoma cells. In turn, we demonstrate that MIR211-5p and MIR328-3p regulation of AURKB plays a crucial role in human nevus formation and that their loss permits progression to melanoma.

Results:

Identification of nevus-enriched microRNAs

We sought to characterize a miRNA program specifically expressed in nevi, as compared to healthy melanocytes or melanoma arising from nevi (Fig. 1A). To first identify miRNAs down-regulated during transformation, we analyzed small RNA-sequencing from a previously established cohort of nevus with adjacent melanoma. Melanocytic nevus and melanoma portions of each tissue section were isolated and subjected to targeted exon, mRNA, and small RNA sequencing (33) (34) (Fig. 1B). For each case, the nevus component was phylogenetically confirmed as a precursor to the adjacent melanoma (33). All lesions shared the $BRAF^{V600E}$ driver mutation. We performed differential expression analysis using the DESeq2 *R* package (35) to determine which microRNAs consistently presented altered expression in the melanomas as compared to the precursor nevi. The analysis revealed a cohort of microRNAs exhibiting elevated expression in the nevus tissue, but down-regulated in the adjacent melanoma tissue, including MIR125B-5p, MIR100-5p, MIR328-3p, MIR211-3p, MIR125A-5p, and MIR211-5p (each p-value adjusted for multiple test correction of <0.05) (Fig. 1C). These observations are consistent with previous studies that have identified MIR125B-5p, MIR100-5p, and MIR211-5p as enriched in nevus tissue as compared with adjacent melanoma (32) (36) (37).

To probe for nevus-specific microRNA expression, as compared to normal human melanocytes, we next isolated melanocytes from fresh biopsies of long-standing nevi with no history of morphological change (n = 6) or healthy human skin with no visible melanocytic neoplasia (n = 8) (Fig. 1D-E). Sanger sequencing confirmed that melanocytes from healthy skin had two wildtype BRAF alleles while nevus melanocytes were heterozygous for the mutant $BRAF^{V600E}$ allele (T1799A) (Fig. 1F). We then performed small- RNA sequencing on these samples. Differential expression analysis identified MIR125B-5p, MIR100-5p, MIR328-3p and MIR211-5p as increased in $BRAF^{V600E}$ nevus melanocytes vs. $BRAF^{WT}$ ($p<0.05$) (Fig. 1G). Taken together, these results suggest these miRNAs form part of a nevus-specific transcriptome that increase in expression with the establishment of the nevus state, then decrease upon transition to melanoma.

MIR211-5p and MIR328-3p induce growth arrest in human melanocytes.

To better characterize the effects of nevus-specific miRNAs on human melanocyte proliferation, we nucleofected primary human melanocytes with RNA mimics corresponding to the mature sequences of MIR125B-5p, MIR100-5p, MIR328-3p and MIR211-5p, as well as non-targeting control mimics, and assayed proliferation over 7 days. Nucleofection of MIR211-5p or MIR328-3p each led to diminished melanocyte proliferation in comparison to the non-targeting control (* = $p<0.05$) (Supplementary Fig. S1A). To validate specificity and potency of each mimic, we generated dual fluorescence reporters of MIR211-5p and MIR328-3p function (Supplementary Fig. S1B). When co-transfected with the targeting microRNA mimics and analyzed via flow cytometry, we observed a uniform inhibition of reporter expression, consistent with subtle translational inhibition expected from microRNA expression (Supplementary Fig. S1C).

To determine whether the proliferation defect was due to growth restriction or increased cell death, we monitored the effects of MIR211-5p and MIR328-3p on normal melanocyte

behavior using digital holographic cytometry (DHC). DHC is a form of quantitative phase imaging (QPI) that permits long-term live imaging and assessment of cell division and death with single cell resolution (38). We conducted DHC of nucleofected melanocytes over the course of 72 hours beginning at day 4 post-nucleofection. MIR211-5p and MIR328-3p overexpression induced a dramatic decrease in melanocyte proliferation in comparison to the non-targeting microRNA control (Fig. 2A). Single-cell analysis revealed only 32.9% and 25.1% of MIR211-5p or MIR328-3p expressing melanocytes divided between day 4 and 5 post-nucleofection, as compared to 85.9% of control cells (Fig. 2B). Growth arrested cells retained the appearance of healthy melanocytes, and the DHC analysis yielded no evidence of cell death (Supplementary Fig. S2A). Growth arrest continued for 6-7 days (Fig. 2C-D). EdU uptake decreased with increasing concentration of MIR211-5p and MIR328-3p mimic 4 days post-nucleofection, further indicating cell division was compromised in human melanocytes following MIR211-5p or MIR328-3p nucleofection (Fig. 2E). Corroborating these observations, cell cycle profiling demonstrated a consistent increase in the number of cells accumulating in S or G2/M phase of the cell cycle between days 3 and 7 following microRNA overexpression (Fig. 2F and 2G). In contrast, co-staining with propidium iodide and annexin V antibody 4 days post-nucleofection revealed no significant differences in the percentage of apoptotic melanocytes (Supplementary Fig. S2B). Taken together, we conclude that over-expression of MIR211-5p and MIR328-3p in human melanocytes induces a proliferative arrest in the G2/M phase of cell cycle.

Endogenous MIR328-3p and MIR211-5p contribute to BRAF^{V600E}-induced growth arrest

Our microRNA profiling of normal and nevus melanocytes and adjacent melanoma showed that MIR211-5p and MIR328-3p were enriched specifically in nevi. Ectopic expression of BRAF^{V600E} has been previously shown to induce growth arrest in human melanocytes (13). As ectopic expression of MIR211-5p and MIR328-3p also induce growth arrest, we reasoned

that endogenous expression of these microRNAs might contribute to $BRAF^{V600E}$-induced growth arrest. To test whether inhibition of endogenous MIR211-5p and MIR328-3p expression is sufficient to rescue $BRAF^{V600E}$-induced growth arrest, we leveraged a doxycycline inducible $BRAF^{V600E}$ system (di$BRAF^{V600E}$) (14). We generated low passage human melanocytes expressing di$BRAF^{V600E}$ and exposed cells to doxycycline. Western blot analysis showed that the transduced melanocyte population expressed increasing levels of $BRAF^{V600E}$ and ERK 1/2 phosphorylation when exposed to increasing concentrations of doxycycline (Fig. 3A). As expected, the induction of $BRAF^{V600E}$ decreased proliferation in melanocytes from three separate donors (Fig. 3B). Cell cycle analysis revealed a dose-responsive increase in the G2/M phase arrest, similar to the miRNA overexpression (Fig. 3C). We were initially surprised by this result, as BRAF-driven G1 phase arrest has been reported, but closer inspection of these previously published data revealed an unappreciated G2/M phase arrest, as well (13) (39).

To determine whether MIR211-5p or MIR328-3p were necessary effectors of $BRAF^{V600E}$-induced growth arrest in human melanocytes, we inhibited MIR211-5p and MIR328-3p in $BRAF^{V600E}$ melanocytes using two approaches. First, we nucleofected di-$BRAF^{V600E}$ melanocytes with LNA microRNA inhibitors and assayed for Edu incorporation after 4 days. In the presence of a non-targeting control inhibitor, induction of $BRAF^{V600E}$ decreased Edu uptake by 7% ($p<0.01$). In contrast, in the presence of inhibitors targeting MIR211-5p or MIR328-3p, there was no significant decrease in mean EdU uptake in melanocytes regardless of $BRAF^{V600E}$ expression (Fig. 3D). As an alternative method to inhibit each microRNA, we generated di-$BRAF^{V600E}$ melanocyte lines that constitutively expressed a microRNA sponge containing seven MIR211-5p or MIR328-3p binding sites and mCherry under control of independent promoters (Fig. 3E). We then conducted a competition assay between mCherry positive (sponge-expressing) and mCherry negative melanocytes. After five days of exposure to doxycycline, the mCherry population of cells expressing control sponge remained at constant, whereas the mCherry population of cells expressing sponges to MIR211-5p or MIR328-3p increased by

44.3% and 21.0%, respectively. Taken together, these results suggest that MIR211-5p and MIR328-3p independently contribute to $BRAF^{V600E}$-mediated growth arrest in human melanocytes.

AURKB and GPR3 inhibition contributes to $BRAF^{V600E}$-induced growth arrest

Previous studies demonstrated that comprehensive characterization of microRNA targets can elucidate novel mechanisms in development and cancer progression (29) (30) (31) (32). Having identified MIR211-5p and MIR328-3p as upregulated in human $BRAF^{V600E}$ nevus melanocytes and contributors to $BRAF^{V600E}$-induced growth arrest, we next investigated the genetic networks regulated by MIR211-5p and MIR328-3p that converge to restrain melanocyte proliferation. We nucleofected normal human melanocytes with MIR211-5p, MIR328-3p, or non-targeting microRNA control mimics. Four days post nucleofection, we harvested total RNA from each sample and performed high-throughput mRNA sequencing. Computationally predicted targets of MIR211-5p and MIR328-3p were enriched among the genes down-regulated by each mimic respectively (Fig. 4A and 4B). The majority of these targets exhibited 2-fold or less expression reduction, consistent with the established models of microRNA targeting on transcript levels.

To determine whether any of the downregulated transcriptional targets of the MIR211-5p or MIR3238-3p contribute directly to the growth arrest microRNA phenotype, we performed a small interfering RNA (siRNA) screen against each target in normal human melanocytes. We tested a total of 131 down-regulated predicted targets of MIR211-5p and MIR328-3p. Of the siRNAs tested, 86 inhibited predicted targets of MIR211-5p, 23 inhibited predicted targets of MIR328-3p, and 6 inhibited predicted targets of both microRNAs (Supplementary Table S1). The effect of each siRNA pool on EdU incorporation was compared to that of six controls: no mimic, a non-targeting siRNA control (Scramble 1), 2 non-targeting microRNA controls (Scramble 2 and Scramble 3), and MIR211-5p and MIR328-3p mimics. Knockdown of 62 of the

131 predicted target genes resulted in EdU uptake significantly less than that of the siControl ($p<0.05$), though few induced changes as significant as the microRNA mimics themselves ((Fig. 4C). These observations are consistent with previous reports that knockdown of individual genes in a microRNA target network can only partially phenocopy overexpression of a microRNA (30).

To further narrow the scope of our study, we focused on genes that were down-regulated by both MIR211-5p and MIR328-3p and whereby knockdown significantly impaired EdU incorporation. We reasoned such genes represent potential network nodes where the MIR211-5p and MIR328-3p target networks converge. We identified AURKB and G-protein coupled receptor 3 (GPR3) as genes with significantly decreased expression upon expression of either microRNA (Fig. 5A). AURKB is predicted to be targeted by both MIR211-5p and MIR328-3p, whereas GPR3 is a predicted target of MIR328-3p only (Fig. 5B). To investigate whether AURKB or GPR3 inhibition is involved in the microRNA-induced growth arrest phenotype, we generated lentiviral constructs that expressed each gene, but lacked the predicted microRNA binding sites (Fig. 5C and 5D). Human melanocytes stably expressing each gene were nucleofected with MIR211-5p, MIR328-3p, or a non-targeting control. We assayed proliferation over 7 days and found that overexpression of AURKB and GPR3 rescued rescued the MIR211-5p induced growth defect (Fig. 5E). Likewise, AURKB overexpression partially rescued the MIR328-3p induced growth arrest, whereas GPR3 overexpression did not ameliorate the phenotype.

To determine whether AURKB or GPR3 expression could rescue the $BRAF^{V600E}$-induced growth arrest in human melanocytes, we overexpressed either AURKB, GPR3, or zsGreen transgenes in human melanocytes previously transduced with the di-$BRAF^{V600E}$ transgene. In the absence of doxycycline- induced $BRAF^{V600E}$ expression, AURKB increased melanocyte proliferation (Fig. 5F). When $BRAF^{V600E}$ was expressed, AURKB rescued proliferation. In contrast, GPR3 expression decreased melanocyte proliferation. Interestingly, when $BRAF^{V600E}$

was expressed, GPR3-expressing cells did not further decrease proliferation (Fig. 5F). To validate the finding that AURKB could rescue $BRAF^{V600E}$-induced growth arrest *in vitro*, we asked whether AURKB was sufficient to restore proliferation to growth arrested human nevi. We transduced non-proliferating nevus melanocytes from three independent donors with lentivirus harboring AURKB and mCherry at low MOI. QPI for 90 hours post-infection demonstrated that nevus melanocytes that expressed mCherry (and therefore AURKB) significantly increased proliferation in comparison to mCherry negative nevus melanocytes (Fig. 5G). These results further suggest that inhibition of AURKB by MIR211-5p and MIR328-3p is essential for the $BRAF^{V600E}$-induced growth arrest in human melanocytes.

Melanoma Growth Requires AURKB Expression

Taken together, our results demonstrate that $BRAF^{V600E}$ nevus melanocytes express increased levels of MIR211-5p and MIR328-3p, and that these microRNAs contribute to growth arrest through inhibition of AURKB and GPR3. If true, we would expect elevated expression of these genes in melanoma as compared to nevi. Transcriptional profiling of nevi (n = 11) and adjacent melanoma (n = 12) from human FFPE tissue revealed that AURKB and GPR3 transcripts are significantly upregulated in melanoma in comparison to nevi – an inverse expression pattern of MIR211-5p and MIR328-3p (Fig. 6A). Immunohistochemistry (IHC) of human nevus (n = 11) and melanoma (n = 11) sections further demonstrated that AURKB and GPR3 expression is upregulated in melanomas relative to nevi (Fig. 6B). If upregulation of either gene were also essential for melanoma growth, we would further expect that inhibition would revert $BRAF^{V600E}$ melanoma cells to a growth-arrested state. Selective inhibitors of AURKB, but not GPR3, have been described. Two $BRAF^{V600E}$ human melanoma cultures – one established line (501MEL) and one derived from a low passage patient-derived xenograft tumor (HCIMel019) – were therefore treated with the selective AURKB inhibitor, Barasertib (40). Both

cultures were highly sensitive to the compound, consistent with a previous report (Fig. 6C) (41). Live DHC imaging revealed no evidence of cell death, but rather growth arrest coupled to significantly increased cell volume, consistent with known functions of AURKB (Fig. 6D-E).

Discussion:

A long-standing question in the field of melanoma biology asks: how are nevi formed? A single mutation – $BRAF^{V600E}$ – drives temporary proliferation followed by subsequent growth arrest, but the mechanisms that underlie this bi-phasic phenotype remain opaque. Equally perplexing is the conditional nature of growth arrest induction, wherein incompletely excised nevi can regrow to their former dimensions (17), or established nevi can erupt in response to external stimuli (18). The mechanisms that permit these events are as ambiguous as nevogenesis itself and require that the growth-arrest phenotype be both recurrently plastic and durable. Such reversible characteristics are more likely to be associated with environmental or transcriptional changes, rather than genetic. Here we identified two microRNAs that are elevated specifically in growth-arrested nevi and are both necessary and sufficient for $BRAF^{V600E}$-induced growth arrest *in vitro*. The microRNAs are downregulated, and their target expression increases in melanoma arising from nevi. Previous studies using melanoma cell lines representative of the advanced disease have identified MIR211-5p as either a tumor suppressor or an oncomir, dependent on context (32) (42) (43) (44) (45) (46) (47) (48). Our data demonstrate that in the context of primary human melanocytes, the transcriptional activation of MIR211-5p and MIR328-3p are at least partially responsible for nevus-associated growth arrest and that melanoma initiation from nevi requires their subsequent suppression.

Our data provide evidence that increased expression of MIR211-5p and MIR328-3p represent intracellular events that complement previously reported transcriptional changes required to establish and maintain growth arrest in nevus melanocytes. In particular, the genes

$p16^{INK4A}$ and $p15^{INK4B}$ are potently upregulated in response to $BRAF^{V600E}$ signaling and thought to contribute to nevus-associated growth arrest (13) (14) (15). Like MIR211-5p and MIR328-3p, expression of both genes can induce melanocyte growth arrest *in vitro* and are frequently lost during transformation to melanoma. However, in contrast to inhibition of MIR211-5p and MIR328-3p, inhibition or genetic ablation of the *CDKN2A* locus does not rescue $BRAF^{V600E}$ induced growth arrest (13) (14) (15) (49) (50). Similarly, deletion of the locus does not prevent nevogenesis in mouse models (51) (52). Another important distinction is the phase of the cell cycle regulated by each gene. Exogenous $BRAF^{V600E}$ expression induces both G0/G1 and G2/M growth arrest while $p16^{INK4A}$ and $p15^{INK4B}$ each inhibit CDK4/6-Cyclin D phosphorylation of RB, leading to a G0/G1 phase cell cycle arrest (13) (39) (53) (54). Conversely, MIR211-5p and MIR328-3p block cell cycle progression through the G2/M phase. Taken together, these observations suggest that microRNA-mediated inhibition of cytokinesis and CDKi-inhibition of cell cycle entry represent two complimentary mechanisms that each contribute to the initiation and the maintenance of growth arrest. Restriction across multiple stages of the cell cycle would enhance the durability of growth arrest in melanocytic nevi, further explaining why so few nevi transform to malignant disease over the lifespan of the individual. The upregulation of multiple cell cycle checkpoints downstream of $BRAF^{V600E}$ may also help explain the difficulties in determining a single phase of the cell cycle in which nevus cells are growth-arrested. Indeed, the extent of $p16^{INK4A}$ expression varies across nevus specimens, ranging from no expression, to mosaic or uniform expression (55)

We identified expression of MIR211-5p and MIR328-3p as a cell-intrinsic mechanism that restrains nevus cell proliferation without the need for further genetic alterations. However, an open question remains regarding the upstream mechanism regulating these microRNAs. We favor a “two-factor” model, whereby increased expression requires both $BRAF^{V600E}$ and activation of a second signaling pathway. In this model, melanocytes that have acquired $BRAF^{V600E}$ would proliferate rapidly until the second pathway, and consequently MIR211-5p and

MIR328-3p, is activated. MIR211-5p has previously been reported to be a transcriptionally regulated by both MITF (32), and UV exposure (56) . Future studies determining how these microRNAs are regulated in $BRAF^{V600E}$ nevus cells might identify additional therapeutic targets for nevus reduction or melanoma prevention.

Regardless of the cause of their expression, analysis of the mechanism of microRNA action, which is pleiotropic and characterized by the simultaneous regulation of networks of target genes, has proven a valuable system for probing the mechanisms of cellular transitions (29) (30) (31). In this study, we demonstrate that MIR211-5p and MIR328-3p converge on AURKB mRNA, the depletion of which is necessary to establish both the microRNA-induced growth arrest and $BRAF^{V600E}$-induced growth arrest in human melanocytes. While AURKB is clearly essential to MIR211-5p and MIR328-3p- mediated proliferation arrest, we recognize that AURKB likely represents one of many MIR211-5p and MIR328-3p targets that contribute to $BRAF^{V600E}$-induced growth arrest in melanocytic nevi. Indeed, data from our siRNA experiment suggest that depletion of multiple targets each phenocopies growth arrest in melanocytes. Previous studies have identified KCNMA1, TGFBR1, TGFBR2, IGF2R, NFAT5, NUAK1, and EDEM1 as MIR211-5p targets in advanced melanoma lines (32) (42) (43) (45) (48). Although we consider the growth suppressive effects of the microRNAs to be the summation of target gene network regulation, it is notable that ectopic AURKB expression on its own was capable of restoring proliferation in previously growth-arrested patient-derived nevus cultures, suggesting this gene is a critical downstream signaling node of these microRNAs in this context. These observations corroborate a previous report that AURKB inhibition is an effective therapy in pre-clinical mouse melanoma models (41), and support further development of AURKB inhibitors as a potential adjuvant or therapeutic candidate.

Acknowledgments:

We acknowledge the use of the HCI Shared Resources for Research Informatics (RI), Cancer Biostatistics (CB), High-Throughput Genomics and Bioinformatics Analysis (GBA), and the Biorepository and Molecular Pathology (BMP) Research Histology Section supported by P30CA042014 awarded to HCI from the National Cancer Institute. This work was supported by NIH awards DP5 OD019787 (to RLJ) and NCI 5F31CA236377 (to ASM).

Author Contributions:

Andrew S. McNeal: Investigation, Formal analysis, Writing – original draft, Visualization, Funding acquisition; Rachel L. Belote: Methodology, Resources, Writing – review & editing; Hanlin Zeng: Methodology, Investigation, Validation, Writing – review & editing; Kendra Barker: Investigation; Rodrigo Torres: Formal analysis; A. Hunter Shain: Data curation, Writing – review & editing; Robert Andtbacka, Writing – review & editing: Resources; Sheri Holmen: Conceptualization; David H Lum: Conceptualization, Writing – review & editing; Timothy H McCalmont: Resources; Matthew W Van Brocklin: Conceptualization; Maria Wei: Resources, Writing – review & editing; Ursula E. Lang: Investigation, Resources, Writing – review & editing; Robert L. Judson-Torres: Conceptualization, Formal analysis, Investigation, Writing – original draft; Visualization, Supervision, Funding acquisition.

Materials and Methods:

RNA sequencing from FFPE tissue and analysis

We previously established a cohort of melanoma specimens presenting with an intact adjacent benign nevus (33). All cases had been retrieved from the UCSF Dermatopathology archive as formalin-fixed paraffin-embedded (FFPE) tissue blocks. Histopathologically distinct areas were independently evaluated by a panel of 5-8 dermatopathologists for staging and genotyped (33). Distinct tumor areas were manually micro-dissected with a scalpel under a dissection scope

from unstained tissue sections following the guidance of a pathologist in order to limit stromal cell contamination. Target exon sequencing, phylogenetic analysis, and RNA and small RNA sequencing of each tumor area were previously described (33) (34) (phs001550.v2.p1). For this study, fifteen different areas (8 malignant and 7 benign) from seven cases were selected based upon BRAF status and confidence of diagnosis. After adaptor sequences were removed, small RNA-seq reads were aligned to a human reference (hg37) with Bowtie (57) and then small RNA reference groups (miRBase21) were counted. Differential expression analysis was performed from feature counts using DESeq2 (35) with p-values adjusted for multiple testing with the Benjamini-Hochberg method (p-adj). Previously published messenger RNA sequencing datasets from *Shain et al. 2018* (33) produced from these samples were re-analyzed here with DESeq2.

RNA sequencing from cultured normal and human nevus melanocytes

MicroRNA sequencing libraries were constructed with the TailorMix Small RNA Library Preparation Kit (SeqMatic, CA) from total RNA extracted from human melanocytes using TRIzol Reagent (Thermo Fisher Cat. # 15596-026) and purified of melanin with the RNeasy Power Clean Pro Cleanup Kit (Qiagen Cat. # 13997-50). Sequencing was performed on the Illumina HiSeq2500 platform at single-end 50bp. Processing, alignment, and analysis of the reads were conducted as described above.

For mRNA sequencing of melanocytes containing microRNA mimics, synthesized mature miRNAs (Dharmacon) were nucleofected into human melanocytes as described below. Four days post-nucleofection, total RNA was collected from biological quadruplicates with TRIzol Reagent (Thermo Fisher Cat. # 15596-026). 150bp paired end sequencing was then conducted on mRNA by GeneWiz. After adaptor sequences were removed, reads were aligned to a human

reference (hg37) with Bowtie2 and HTSeq was used to count reads. Differential expression analysis was performed from normalized counts using EdgeR and LimmaVoom (58) with p-values adjusted for multiple testing by the Benjamini-Hochberg method (p-adj).

Cell Derivation and Culture

Benign human melanocytic nevi were excised with informed consent from patient donors at the University of California San Francisco Dermatology clinic (San Francisco, CA) according to an Institutional Review Board- approved protocol. Patient studies were conducted in accordance with the Declaration of Helsinki. The tissue samples were microdissected to isolate nevus from surrounding normal tissue. Nevus tissue was then mechanically separated into pieces and enzymatically dissociated in a 1:1:1 mixture of DMEM:Dispase:Collagenase (DMEM Thermo Fisher Cat # 10569044 : Dispase : Collagenase) for 1 hour at 37ºC. Melanocytes were further isolated from epidermal keratinocytes and fibroblasts by selective trypsinization and 5- day exposure to 10µg/mL G418 (Geneticin). BRAF status of nevus-derived melanocytes was confirmed via sanger sequencing (Quintarabio) using the primer (BRAF forward: 5'- GCA CGA CAG ACT GCA CAG GG -3'; BRAF reverse: 5'- AGC GGG CCA GCA GCT CAA TAG -3'). BRAFWT (normal) human melanocytes were isolated from de-identified and IRB consented neonatal foreskins. Foreskin tissue was incubated overnight at 4ºC in Dispase and epithelia were mechanically separated from the dermis the following morning using forceps. The epithelial tissue was minced and incubated in trypsin for 4min at 37ºC. Trypsin was quenched with soybean trypsin inhibitor and tissue was centrifuged at 500xg for 5min at room temperature. The supernatant was aspirated and the cell/tissue pellet was resuspended in Melanocyte medium (ThermoFisher, M254500) supplemented with HMGS (ThermoFisher, S0025) and plated in low volume to promote cell adherence.

The 501Mel human melanoma line (Gift from Dr. Boris Bastian, CVCL_4633) were cultured in RPMI media with 10% Fetal Bovine Serum (FBS), 1% Penicillin-Streptomycin (Pen-Strep), 1% L-Glutamine (L-Glut), and 1% Non-Essential Amino Acid (NEAA) cell culture supplement.
The human melanoma cell line HCIMel019 was derived from patient-derived xenograft (PDX) tumors propagated in mice. An HCIMel019 (P2) subcutaneous tumor was resected from a mouse and minced in tissue digestion buffer consisting of 100μM HEPES (Gibco, 15630-080), 5% FBS (DENVILLE, FB5001-H), 20μg/ml gentamicin (Gibco, 15710-064), 1x insulin (Gibco, 51500-056), and 1mg/ml collagenase IV (Gibco, 17104-019) in DMEM (Gibco, 11965-092). The tumor slurry was digested overnight in 37˚C with gently shaking. The cells were filtered through a 100uM pore size filter (Falcon, 352360) and red blood cells were removed with RBC lysis buffer consisting of 0.5M EDTA, 0.5M KHCO3 (Sigma, 237205), and 5M NH4CL (Sigma, A9434). The remaining cells washed with PBS and cultured in a humidified incubator at 37C and 5% CO2 in Mel2 media consisting of 80%MCDB153 (Sigma, M7403), 20% L15 (Gibco, 11415-064), 2% (DENVILLE, FB5001-H), 1.68mM CaCL (Sigma, C4901), 1x insulin (Gibco, 51500-056) 5ng/mlEGF 5ng/ml (Sigma Aldrich, E9644), 15μg/ml Bovine Pituitary Extract (Gibco 13028-014), and 1x Pen/strep (Gibco, 15070-063).

Mimic Nucleofection

Human melanocytes were trypsinized, quenched with DMEM + 10% FBS + 1% antibiotic/antimyotic and centrifuged at 300xg. The resulting cell pellet was resuspended in R Buffer at a concentration of 10,000 cells/μL and 10μL nucleofected with mature miRIDIAN microRNA mimics (Dharmacon) (hsa-MIR211-5p C-300566-03-0005, hsa-MIR328-3p C-300695-03-0005, MIRControl 1 CN-001000-01-05, MIRControl 2 CN-002000-01-05) with a final concentration of 4μM. microRNA LNA inhibitors (Qiagen) (anti-hsa-MIR211-5p YI04103166-ADC, anti-hsa-MIR328-3p YI04101608-ADC, anti-MIRControl 1 YI00199006-ADC, anti-

MIRControl 2 YI00199007-ADC) were also nucleofected with a final concentration of 4μM nucleofected using the NEON Transfection System and protocol (Thermo Fisher Cat. # MPK5000).

Generation of Lentiviral vectors

pTRIPZ-diBRAFV600E was previously described (a gift from Todd Ridky) (14). pLVX-AURKB (Addgene #153316) and pLVX-GPR3 (Addgene #153317) were generated by subcloning the respective human cDNA (from Addgene #100142 and #66350) into the [MluI and BamHI sites] of the pLVX-Che-hi3 vector (a gift Sanford Simon) (Takacs et al. 2017). pLVX-anti-MIR211-5p (Addgene #153318), pLVX-anti-MIR328-3p (Addgene #153319), and pLVX-Che-zsGreen (Addgene #153320) were generated by inserting zsGreen with or without a 3'UTR into the [MluI and XbaI sites] of the pLVX-Che-hi3 vector. The 3'UTRs contained 7 tandem microRNA binding sites to both report and inhibit microRNA function, as previously described (30). ZsGreen was subcloned from pHIV-zsGreen (a gift from Bryan Welm & Zena Werb (Addgene plasmid # 18121) (59).

Lentiviral transduction

$2.75x10^6$ HEK293T cells were plated in 10cm tissue culture treated dishes and grown for approximately 24 hours in DMEM supplemented with 10% FBS and 1% antibiotic-antimycotic. For each 10cm plate, 3.3μg of pMLV-GagPol and 1.7ug of pVSV-G packaging plasmids were added to 500μL of jetPRIME buffer (Polyplus catalog # 712-60) and briefly vortexed to mix. 5μg of lentiviral vector and 20μL of jetPRIME transfection reagent were then added to the jetPRIME buffer and the mixture was briefly vortexed. The mixture was then incubated for 10min at room temperature and added to the HEK293T culture media. 48 hours post-transfection, viral supernatant was collected and filtered using 0.45μm syringe filters (Argos). Human

melanocytes seeded at $1.0x10^5$ – $2.0x10^5$ cells/well density in 6-well plates were then incubated in viral supernatant in the presence of 10µg/mL polybrene and centrifuged at 300xg for 60 min at room temperature. Transduced melanocytes were incubated for 15min at 37ºC after which the viral supernatant was removed and replaced with growth media. Transduced cells were then either selected with puromycin (1µg/mL for 5 days) or sorted for mCherry expression using a BD FACSAria II. In some experiments, cells expressing pTRIPZ-diBRAFV600E were treated with doxycycline at indicated concentrations.

Live Quantitative Phase Imaging

Digital holographic cytometry was performed using HoloMonitor M4 imaging cytometers (Phase Holographic Imaging, Lund, Sweden) and analyzed for cell proliferation, volume and death using HStudio (v2.6.3) as previously described in Hejna et al. 2017 (38). For normal human melanocyte proliferation experiments, cells were seeded into 6-well culture plates (Sarstedt, 83.3920) at 100,000 cells per well and either live-imaged in a standard mammalian cell incubator or serially imaged at different days as indicated. For dose response curves, 60,000 501Mel cells or 150,000 HCIMel019 cells were plated per well. The next day, media was replaced with media containing indicated concentrations of barasertib (AURKB inhibitor; AZD1152-HQPA | AZD2811) obtained from Selleckchem.com (Catalog No. A1147 – 5 mg) and cells were imaged for 48-72 hours. Live quantitative phase imaging coupled with fluorescent imaging was conducted using the Livecyte platform (Phasefocus, Sheffield, UK).

EdU assays

Normal human melanocytes were nucleofected with microRNA mimics, LNA microRNA inhibitors, or infected with lentiviral vectors (as above) and seeded in 48-well plates at a density of 50,000 cells/well. 4 days post-seeding EdU was added to culture media at a final concentration of 10µM. 24 hours after the addition of EdU, EdU media was removed and cells

were stained for EdU incorporation and nuclei using the Click-iT EdU Imaging Kit (Thermo Fisher Cat. # C10337) and protocol. Images of EdU and nuclei staining were taking using the Evos FL microscope and quantified using FIJI.

microRNA qRT-PCR

Total RNA was extracted from melanocytes using TRIzol Reagent (Thermo Fisher Cat. # 15596-026) and purified of melanin with the RNeasy Power Clean Pro Cleanup Kit (Qiagen Cat. # 13997-50). RNA concentrations were established by NanoDrop. microRNAs were then converted to cDNA using TaqMan Advanced miRNA Assays (Thermo Fisher Cat. # A25576). Quantitative PCR was carried out in triplicate using the TaqMan Fast Advanced Master Mix (Thermo Fisher Cat. # 4444557) and TaqMan probes corresponding to each microRNA of interest on an Applied Biosystems 7900HT machine. MIR191-5p and MIR26a-5p were used as reference controls and the delta-delta CT method was used to approximate gene expression.

Western Blotting

Protein was collected using RIPA Buffer (Thermo Fisher Cat. # 89901) supplemented with HALT Protease Inhibitor (Thermo Fisher Cat. # 87786). Protein extracts were mixed with NuPAGE LDS Sample Buffer (ThermoFisher Cat. # NP0007), NuPAGE Sample Reducing Agent (ThermoFisher Cat. # NP0004) and heated for 10 min at 90 °C. Protein was resolved on NuPAGE Novex 4–12% Bis-Tris Protein Gels, 1.0 mm, 15-well (ThermoFisher Cat. # NP0323BOX) and transferred using a Mini-Trans-Blot Cell onto 0.22µm PVDF membranes (ThermoFisher Cat. # 88520). Membranes were blocked with Membrane Blocking Solution (ThermoFisher Cat. # 000105) for 20 min. at room temperature (22 °C). The membranes were then incubated overnight at 4 °C with primary antibodies at the following dilutions: anti-HSP90 (CST Cat. # 4874) 1:1000, anti-BRAFV600E (Spring Bioscience Corp Cat. # E19292) 1:1000, anti-phosphoERK1/2 (CST Cat. # 4970) 1:1000, anti-AURKB (Abcam ab2254) 1:1000. The

membranes were then washed four times with PBS and 0.5% Tween20 (TBST) and incubated with horseradish peroxidase-conjugated secondary antibody 1:2000 for 30 min. at room temperature. The membranes were then washed four times with TBST and were visualized with Lumina Forte Western HRP substrate (Millipore Cat. # WBLUF0500).

Cell cycle and apoptosis profiling

Melanocytes were trypsinized with 0.05% Trypsin (Thermo Fisher Cat# 25300120) and quenched with DMEM + 10% FBS + 1% antibiotic/antimycotic. Cells were centrifuged at 1000 rpm for 5 min. The supernatant was aspirated, and cells were resuspended in ice cold 1X PBS with 3% BSA. Cells were centrifuged for additional 1 min and cells were resuspended in 500µL of ice cold 70% ethanol. Cells were then fixed for 1 hr at 4ºC. After fixation, cells were centrifuged for 5 min at 1000rpm and washed 1X PBS with 3% BSA. Cells were resuspended in 200µL of 1X PBS with 0.5mg/mL propidium iodide (PI) (BioLegend Cat# 421301) and incubated in the dark at room temperature for 30 min. PI stained cells were analyzed with BD FACs Verse.

Annexin V/PI staining was performed by trpysinizing melanocytes as above. Cells were washed with PBS and resuspended with Annexin V binding buffer (BioLegend Cat# 422201) at a concentration of 1X10^6 cell/mL. 5µL of APC Annexin V antibody (BioLegend Cat# 640919) and 10µL of PI were added. Cells were gently vortexed and incubated 15min at room temperature in the dark. 400µL of Annexin V Binding Buffer was added and samples were analyzed on the BD FACs Verse.

Human nevus and melanoma tissue Immunohistochemistry

The clinical samples used in the study were procured with IRB approval from the archives of the UCSF Dermatopathology and Oral Pathology Service. All samples, 11 melanoma and 11

melanocytic nevi, had received prior pathological diagnosis by board-certified dermatopathologists (THM and UEL), were de-identified and re-verified histologically (UEL). Tissue was fixed in 10% neutral-buffered formalin, routinely processed, embedded in paraffin, and stained with hematoxylin and eosin. Formalin-fixed paraffin-embedded sections of 4 μm thickness were stained with antibodies specific for AURKB (1:400 dilution, Abcam ab2254) and GPR3 (1:125 dilution, Abnova H00002827-M01). Review of immunohistochemical stains was performed by UEL with semiquantitative grading for GPR3 (0=none; 1=patchy positive; 2=strong positive) and AURKB (0=none; 1=rare positive; 2=scattered positive; 3= frequent positive; 4=many positive).

Data availability

This sequencing data produced in this manuscript is available from GEO (GSE150849).

References:

1. Bastian BC. The Molecular Pathology of Melanoma: An Integrated Taxonomy of Melanocytic Neoplasia. Annu Rev Pathol Mech Dis. 2014;9:239–71.

2. Siegel RL, Miller KD, Jemal A. Cancer statistics, 2020. CA A Cancer J Clin. 2020;70:7–30.

3. Siegel RL, Miller KD, Jemal A. Cancer statistics, 2017. CA: A Cancer Journal for Clinicians. 2017;67:7–30.

4. Gershenwald JE, Scolyer RA, Hess KR, Sondak VK, Long GV, Ross MI, et al. Melanoma staging: Evidence-based changes in the American Joint Committee on Cancer eighth edition cancer staging manual: Melanoma Staging: AJCC 8 th Edition. CA: A Cancer Journal for Clinicians. 2017;67:472–92.

5. Pollock PM, Harper UL, Hansen KS, Yudt LM, Stark M, Robbins CM, et al. High frequency of BRAF mutations in nevi. Nat Genet. 2003;33:19–20.

6. Garnett MJ, Marais R. Guilty as charged: B-RAF is a human oncogene. Cancer Cell. 2004;6:313–9.

7. Robinson W, Lemon M, Elefanty A, Harrison-Smith M, Markham N, Norris D. Human acquired naevi are clonal. Melanoma research. 1998;8:499—503.

8. Yeh I, von Deimling A, Bastian BC. Clonal BRAF Mutations in Melanocytic Nevi and Initiating Role of BRAF in Melanocytic Neoplasia. JNCI: Journal of the National Cancer Institute. 2013;105:917–9.

9. Uribe P, Andrade L, Gonzalez S. Lack of Association between BRAF Mutation and MAPK ERK Activation in Melanocytic Nevi. Journal of Investigative Dermatology. 2006;126:161–6.

10. Aird KM, Zhang G, Li H, Tu Z, Bitler BG, Garipov A, et al. Suppression of Nucleotide Metabolism Underlies the Establishment and Maintenance of Oncogene-Induced Senescence. Cell Reports. 2013;3:1252–65.

11. Di Micco R, Fumagalli M, Cicalese A, Piccinin S, Gasparini P, Luise C, et al. Oncogene-induced senescence is a DNA damage response triggered by DNA hyper-replication. Nature. 2006;444:638–42.

12. Stolz W, Abmayr W, Schmoeckel C, Landthaler M, Massoudy P, Braun-Falco O. Ultrastructural Discrimination Between Malignant Melanomas and Benign Nevocytic Nevi Using High-Resolution Image and Multivariate Analyses. Journal of Investigative Dermatology. 1991;97:903–10.

13. Michaloglou C, Vredeveld LCW, Soengas MS, Denoyelle C, Kuilman T, van der Horst CMAM, et al. BRAFE600-associated senescence-like cell cycle arrest of human naevi. Nature. 2005;436:720–4.

14. McNeal AS, Liu K, Nakhate V, Natale CA, Duperret EK, Capell BC, et al. CDKN2B Loss Promotes Progression from Benign Melanocytic Nevus to Melanoma. Cancer Discovery. 2015;5:1072–85.

15. Zeng H, Jorapur A, Shain AH, Lang UE, Torres R, Zhang Y, et al. Bi-allelic Loss of CDKN2A Initiates Melanoma Invasion via BRN2 Activation. Cancer Cell. 2018;34:56-68.e9.

16. Shain AH, Yeh I, Kovalyshyn I, Sriharan A, Talevich E, Gagnon A, et al. The Genetic Evolution of Melanoma from Precursor Lesions. N Engl J Med. 2015;373:1926–36.

17. King R, Hayzen BA, Page RN, Googe PB, Zeagler D, Mihm MC. Recurrent nevus phenomenon: a clinicopathologic study of 357 cases and histologic comparison with melanoma with regression. Mod Pathol. 2009;22:611–7.

18. Burian EA, Jemec GBE. Eruptive Melanocytic Nevi: A Review. Am J Clin Dermatol. 2019;20:669–82.

19. Funk JO, Schiller PI, Barrett MT, Wong DJ, Kind P, Sander CA. p16INK4a expression is frequently decreased and associated with 9p21 loss of heterozygosity in sporadic melanoma. J Cutan Pathol. 1998;25:291–6.

20. Keller-Melchior R, Schmidt R, Piepkorn M. Expression of the Tumor Suppressor Gene Product p16INK4 in Benign and Malignant Melanocytic Lesions. Journal of Investigative Dermatology. 1998;110:932–8.

21. Reed JA, Loganzo F, Shea CR, Walker GJ, Flores JF, Glendening JM. Loss of Expression of the p16/Cydin-dependent Kinase Inhibitor 2 Tumor. Cancer Research. 55:2713–8.

22. Talve L, Sauroja I, Collan Y, Punnonen K, Ekfors T. Loss of expression of the p16INK4/CDKN2 gene in cutaneous malignant melanoma correlates with tumor cell proliferation and invasive stage. Int J Cancer (Pred Oncol). 74:255–9.

23. Wang Y-L, Uhara H, Yamazaki Y, Nikaido T, Saida T. Immunohistochemical detection of CDK4 and 9 16 ^{INK4} proteins in cutaneous malignant melanoma. Br J Dermatol. 1996;134:269–75.

24. Ebert MS, Sharp PA. Roles for MicroRNAs in Conferring Robustness to Biological Processes. Cell. 2012;149:515–24.

25. Georgantas RW, Streicher K, Luo X, Greenlees L, Zhu W, Liu Z, et al. MicroRNA-206 induces G1 arrest in melanoma by inhibition of CDK4 and Cyclin D. Pigment Cell Melanoma Res. 2014;27:275–86.

26. Nemlich Y, Greenberg E, Ortenberg R, Besser MJ, Barshack I, Jacob-Hirsch J, et al. MicroRNA-mediated loss of ADAR1 in metastatic melanoma promotes tumor growth. J Clin Invest. 2013;123:2703–18.

27. Kanemaru H, Fukushima S, Yamashita J, Honda N, Oyama R, Kakimoto A, et al. The circulating microRNA-221 level in patients with malignant melanoma as a new tumor marker. Journal of Dermatological Science. 2011;61:187–93.

28. Forloni M, Dogra SK, Dong Y, Conte D, Ou J, Zhu LJ, et al. miR-146a promotes the initiation and progression of melanoma by activating Notch signaling. eLife. 2014;3:1–20.

29. Melton C, Judson RL, Blelloch R. Opposing microRNA families regulate self-renewal in mouse embryonic stem cells. Nature. 2010;463:621–6.

30. Judson RL, Greve TS, Parchem RJ, Blelloch R. MicroRNA-based discovery of barriers to dedifferentiation of fibroblasts to pluripotent stem cells. Nat Struct Mol Biol. 2013;20:1227–35.

31. Pencheva N, Tran H, Buss C, Huh D, Drobnjak M, Busam K, et al. Convergent Multi-miRNA Targeting of ApoE Drives LRP1/LRP8-Dependent Melanoma Metastasis and Angiogenesis. Cell. 2012;151:1068–82.

32. Levy C, Khaled M, Iliopoulos D, Janas MM, Schubert S, Pinner S, et al. Intronic miR-211 Assumes the Tumor Suppressive Function of Its Host Gene in Melanoma. Molecular Cell. 2010;40:841–9.

33. Shain AH, Joseph NM, Yu R, Benhamida J, Liu S, Prow T, et al. Genomic and Transcriptomic Analysis Reveals Incremental Disruption of Key Signaling Pathways during Melanoma Evolution. Cancer Cell. 2018;34:45-55.e4.

34. Torres R, Lang UE, Hejna M, Shelton SJ, Joseph NM, Shain AH, et al. MicroRNA Ratios Distinguish Melanomas from Nevi. Journal of Investigative Dermatology. 2020;140:164-173.e7.

35. Love MI, Huber W, Anders S. Moderated estimation of fold change and dispersion for RNA-seq data with DESeq2. Genome Biol. 2014;15:550.

36. Holst LMB, Kaczkowski B, Glud M, Futoma-Kazmierczak E, Hansen LF, Gniadecki R. The microRNA molecular signature of atypic and common acquired melanocytic nevi: differential expression of miR-125b and let-7c: Letter to the Editor. Experimental Dermatology. 2011;20:278–80.

37. Wandler A, Riber-Hansen R, Hager H, Hamilton-Dutoit S, Schmidt H, Nielsen B, et al. Quantification of microRNA-21 and microRNA-125b in melanoma tissue. Melanoma Research. 2017;27:417–28.

38. Hejna M, Jorapur A, Song JS, Judson RL. High accuracy label-free classification of single-cell kinetic states from holographic cytometry of human melanoma cells. Sci Rep. 2017;7:11943.

39. Zhu J, Woods D, McMahon M, Bishop JM. Senescence of human fibroblasts induced by oncogenic Raf. Genes & Development. 1998;12:2997–3007.

40. Helfrich BA, Kim J, Gao D, Chan DC, Zhang Z, Tan A-C, et al. Barasertib (AZD1152), a Small Molecule Aurora B Inhibitor, Inhibits the Growth of SCLC Cell Lines In Vitro and In Vivo. Molecular Cancer Therapeutics. 2016;15:2314–22.

41. Porcelli L, Guida G, Quatrale AE, Cocco T, Sidella L, Maida I, et al. Aurora kinase B inhibition reduces the proliferation of metastatic melanoma cells and enhances the response to chemotherapy. J Transl Med. 2015;13:26.

42. Vitiello M, Tuccoli A, D'Aurizio R, Sarti S, Giannecchini L, Lubrano S, et al. Context-dependent miR-204 and miR-211 affect the biological properties of amelanotic and melanotic melanoma cells. Oncotarget. 2017;8:25395–417.

43. Bell RE, Khaled M, Netanely D, Schubert S, Golan T, Buxbaum A, et al. Transcription Factor/microRNA Axis Blocks Melanoma Invasion Program by miR-211 Targeting NUAK1. Journal of Investigative Dermatology. 2014;134:441–51.

44. Díaz-Martínez M, Benito-Jardón L, Alonso L, Koetz-Ploch L, Hernando E, Teixidó J. miR-204-5p and miR-211-5p Contribute to BRAF Inhibitor Resistance in Melanoma. Cancer Res. 2018;78:1017–30.

45. Golan T, Parikh R, Jacob E, Vaknine H, Zemser-Werner V, Hershkovitz D, et al. Adipocytes sensitize melanoma cells to environmental TGF-β cues by repressing the expression of miR-211. Sci Signal. 2019;12:1–15.

46. Sahoo A, Sahoo SK, Joshi P, Lee B, Perera RJ. MicroRNA-211 Loss Promotes Metabolic Vulnerability and BRAF Inhibitor Sensitivity in Melanoma. Journal of Investigative Dermatology. 2019;139:167–76.

47. Mazar J, Qi F, Lee B, Marchica J, Govindarajan S, Shelley J, et al. MicroRNA 211 Functions as a Metabolic Switch in Human Melanoma Cells. Mol Cell Biol. 2016;36:1090–108.

48. Mazar J, DeYoung K, Khaitan D, Meister E, Almodovar A, Goydos J, et al. The Regulation of miRNA-211 Expression and Its Role in Melanoma Cell Invasiveness. Cheriyath V, editor. PLoS ONE. 2010;5:1–14.

49. Halaban R, Cheng E, Zhang Y, Mandigo CE, Miglarese MR. Release of cell cycle constraints in mouse melanocytes by overexpressed mutant E2F1E132, but not by deletion of p16INK4A or p21WAF1/CIP1. Oncogene. 1998;16:2489–501.

50. Haferkamp S, Tran SL, Becker TM, Scurr LL, Kefford RF, Rizos H. The relative contributions of the p53 and pRb pathways in oncogene-induced melanocyte senescence. Aging. 2009;1:542–56.

51. Damsky W, Micevic G, Meeth K, Muthusamy V, Curley DP, Santhanakrishnan M, et al. mTORC1 Activation Blocks BrafV600E-Induced Growth Arrest but Is Insufficient for Melanoma Formation. Cancer Cell. 2015;27:41–56.

52. Dhomen N, Reis-Filho JS, da Rocha Dias S, Hayward R, Savage K, Delmas V, et al. Oncogenic Braf Induces Melanocyte Senescence and Melanoma in Mice. Cancer Cell. 2009;15:294–303.

53. Zhang HS, Postigo AA, Dean DC. Active Transcriptional Repression by the Rb–E2F Complex Mediates G1 Arrest Triggered by p16INK4a, TGF-ß, and Contact Inhibition. Cell. 1999;97:53–61.

54. Hannon GJ, Beach D. pl5INK4B is a potential effector of TGF-β-induced cell cycle arrest. Nature. 1994;371:257–61.

55. Smith EH, Lowe L, Harms PW, Fullen DR, Chan MP. Immunohistochemical evaluation of p16 expression in cutaneous histiocytic, fibrohistiocytic and undifferentiated lesions. J Cutan Pathol. 2016;43:671–8.

56. Su M, Miao F, Jiang S, Shi Y, Luo L, He X, et al. Role of the p53-TRPM1/miR-211-MMP9 axis in UVB-induced human melanocyte migration and its potential in repigmentation. Int J Mol Med. 2020;4478:1–10.

57. Langmead B, Trapnell C, Pop M, Salzberg SL. Ultrafast and memory-efficient alignment of short DNA sequences to the human genome. Genome Biol. 2009;10:1–10.

58. Law CW, Chen Y, Shi W, Smyth GK. voom: precision weights unlock linear model analysis tools for RNA-seq read counts. Genome Biol. 2014;15:1–17.

59. Welm BE, Dijkgraaf GJP, Bledau AS, Welm AL, Werb Z. Lentiviral Transduction of Mammary Stem Cells for Analysis of Gene Function during Development and Cancer. Cell Stem Cell. 2008;2:90–102.

Figure Legends

Figure 1: Identification of nevus- enriched microRNAs.

(A) Schematic highlighting plastic nature of $BRAF^{V600E}$ nevus- associated growth arrest and putative nevus specific transcriptional program.

(B) H&E of representative nevus to melanoma transition case (4X) with higher magnification insets (20X) of nevus and melanoma portions.

(C) Box-Whisker plots from small-RNA sequencing of transition cases (n = 7 matched biological replicates of nevi and melanoma). P-values calculated by unpaired T Test.

(D) Representative photomicrographs (10X) of normal skin and nevus biopsies.

(E) Human foreskin-derived melanocytes (top) and human nevus-derived melanocytes (bottom) (10X) representative photomicrographs.

(F) Matched sanger sequencing chromatograms for normal (top) and nevus (bottom). T1799 indicated by arrow.

(G) Box-Whisker plots of nevus-enriched microRNA expression in $BRAF^{WT}$ human melanocytes (n= 8 biological replicates) and $BRAF^{V600E}$ human nevus melanocytes (n = 6 biological replicates). P-values calculated by unpaired T Test.

Figure 2: MIR211-5p and MIR328-3p induce growth arrest in human melanocytes.

(A) Representative images from live digital holographic imaging of melanocytes nucleofected with indicated microRNA mimics. Imaging started at 4 days post- nucleofection.

(B) Percent of melanocytes divided between days 4 and 5 post- microRNA mimic nucleofection (4μM) for MIR211-5p (green), MIR328-3p (light blue) vs. MIRControl (dark blue). Digital holographic cytometry.

Line **(C)** and bar **(D)** plots of means and standard deviations of population fold change over 7 days of MIR211-5p and MIR328-3p (4μM) nucleofected melanocytes vs. non-targeting MIRControl.

(E) Percent EdU positive cells 4 days after nucleofection with 1, 2, 4, and 6μM miRNA mimic. (MIR211-5p (green), MIR328-3p (light blue) vs. MIRControl (dark blue), n=3 replicates).

(* = $p < 0.05$, ** = $p < 0.01$, unpaired T test)

(F) Representative histograms of propidium iodide staining as measured by flow cytometry. Percentages reflect percent cells in S or G2/M phases of cell cycle.

(G) Percent cells in S or G2/M phases of cell cycle 7 days post- nucleofection with MIRControl, MIR211-5p, or MIR328-3p. P-values calculated by paired T Test, n=5 biological replicates.

Figure 3: $BRAF^{V600E}$ induced growth arrest requires MIR211-5p and MIR328-3p.

(A) Western Blot analysis of $BRAF^{V600E}$, phospho-ERK1/2 in $diBRAF^{V600E}$ melanocytes in response to increasing concentration of doxycycline. HSP90 was used as a loading control.

(B) Population fold change for $diBRAF^{V600E}$ MCs treated with 62.6 ng/mL doxycycline (paired T Test, n=3 biological replicates).

(C) Percent cells in S or G2/M phases of cell cycle after 7 days exposure to indicated concentrations of doxycycline. (* = $p < 0.05$, paired T Test)

(D) Mean and standard deviation of percent EdU positive $diBRAF^{V600E}$ melanocytes 7 days post-nucleofection with MIRControl, MIR211-5p, or MIR328-3p LNA inhibitors and with (+) or without (-) exposure to doxycycline. (** = $p<0.01$, unpaired T test) (n = 6 biological replicates).

(E) Schematic of expected (top) and actual (bottom) results (mean and standard deviation) for competitive growth assay comparing $diBRAF^{V600E}$ melanocytes grown 13 days with exposure to doxycycline with or without mCherry tagged microRNA sponges. (* = $p < 0.05$, ** = $p<0.005$, *** = $p<0.0005$, unpaired T Test comparing D13 to D1, n=3 replicates)

Figure 4: Identification of MIR211-5p and MIR328-3p mRNA targets.

(A) Volcano plots of mRNA sequencing from n = 4 biological replicates of melanocytes nucleofected with MIR211-5p (left) or MIR328-3p (right) vs. MIRControl. (MIR211-5p predicted targets = green, MIR328-3p predicted targets = light blue).

(B) GSEA analysis comparing predicted MIR211-5p and MIR328-3p target mRNAs to changes in gene expression after nucleofection with indicated mimics compared to nucleofection control.

(C) Mean and standard deviation from n = 3 replicates of percent EdU positive melanocytes harboring knockdown of predicted MIR211-5p (left) or MIR328-3p (right) targets. Dark blue bars represent no mimic (nucleofection) control and three scrambled controls. Green bar represents MIR211-5p and light blue bar represents MIR328-3p.

Figure 5: AURKB and GPR3 inhibition contribute to BRAFV600E-induced growth arrest.

(A) Normalized read counts for AURKB or GPR3 in melanocytes nucleofected with MIRControl (dark blue), MIR211-5p (green), or MIR328-3p (light blue). P-values calculated by Wilcoxon test (n = 4 biological replicates for each condition).

(B) Schematics showing potential binding sites of MIR211-5p and MIR328-3p in the 3' UTRs of AURKB (left) and GPR3 (right).

(C) Western Blot of AURKB expression in human melanocytes with or without lentiviral AURKB overexpression. HSP90 is the loading control.

(D) Representative photomicrographs (20X) of immunofluorescence for GPR3 (green) or (Hoechst) (purple) in human melanocytes with GPR3 lentiviral overexpression (GPR3 OE) or without (Control) over-expression.

(E) Cell number fold change mean and standard deviation for melanocytes overexpressing zsGreen control, AURKB, or GPR3 and nucleofected with MIR211-5p (left) and MIR328-3p (right). P values calculated by type 2 unpaired T Test. (*= $p<0.05$) (n = 6 biological replicates).

(F) Cell number fold change mean and standard deviation for melanocytes transduced with doxycycline inducible BRAFV600E and either ZSGreen control, AURKB, or GPR3, and then treated with (+) or without (-) dox. (p values calculated by unpaired T-Test and compare to ZSGreen (+) or ZSGreen (-) dox respectively *= $p<0.05$) (n = 6 biological replicates).

(G) Experimental design (top left) and representative images capturing dividing nevus melanocyte (bottom left) and quantification (right) of digital holography of human nevus cells infected with low titer AURKB/mCherry lentivirus. (n = 3 biological replicates) (p value calculated by paired T-Test).

Figure 6: AURKB expression promotes melanoma growth.

(A) Normalized read counts for AURKB (left) and GPR3 (right) expression in matched nevi and adjacent melanoma (n = 11 nevi and 12 matched melanomas) (p values calculated by Wilcoxon test).

(B) Representative images (top) and quantification (bottom) of immunohistochemical staining for AUKRB (brown chromagen) and GPR3 (red chromagen) expression in FFPE samples of nevi and melanoma. (n = 11 each group).

(C) Dose response curves for established human melanoma cell line (501MEL) and primary human melanoma culture (HCIMel019) treated with AURKB inhibitor, barasertib.

(D) Representative digital holographic images of HCIMel019 treated with DMSO control or 300 nM barasertib.

(E) Quantification of cell volume 48 hours after treatment with indicated concentrations of barasertib (n=3 replicates, * = p <0.05, ** = p<0.01, unpaired T test).

Supplementary Figure Legends

Supplementary Figure 1: Screening and validation of MIR211-5p and MIR328-3p mimics

(A) Mean and standard deviation for population fold change of melanocytes nucleofected with nevus or melanoma-enriched microRNA mimics compared to non-targeting control (MIRControl) (n = 3 biological replicates) (p values calculated by unpaired TTest * = p<0.05).

(B) Schematic of microRNA sponge constructs, which serve as both reporters and inhibitors of microRNA function. A zsGreen cDNA expressing a 3' UTR with 7 tandem microRNA binding sites is expressed from the CMV promoter, whereas an mCherry that is not under microRNA regulation is expressed from the pGK promoter. After transduction, mCherry positive cells are expected to express the microRNA inhibitor and the ratio of zsGreen to mCherry provides a read-out of functional microRNA expression.

(C) FACS analysis depicting the zsGreen to mCherry ratio of melanocytes transduced with control, MIR328-3p, or MIR211-5p sponges, then nucleofected with MIR328-3p or MIR211-5p

mimics. Physiological functional expression of the microRNAs is predicted to cause a subtle left-shift in the distribution, as observed.

Supplementary Figure 2: MicroRNA mimics do not induce significant cell death

(A) Quantification of the number of dead or dying cells from digital holographic imaging over 72 hours shown in Fig. 1.

(B) Quantification of % Annexin V/PI positive cells. (n = 3 biological replicates). P values indicate one-way ANOVA multiple comparison to MIRControl.

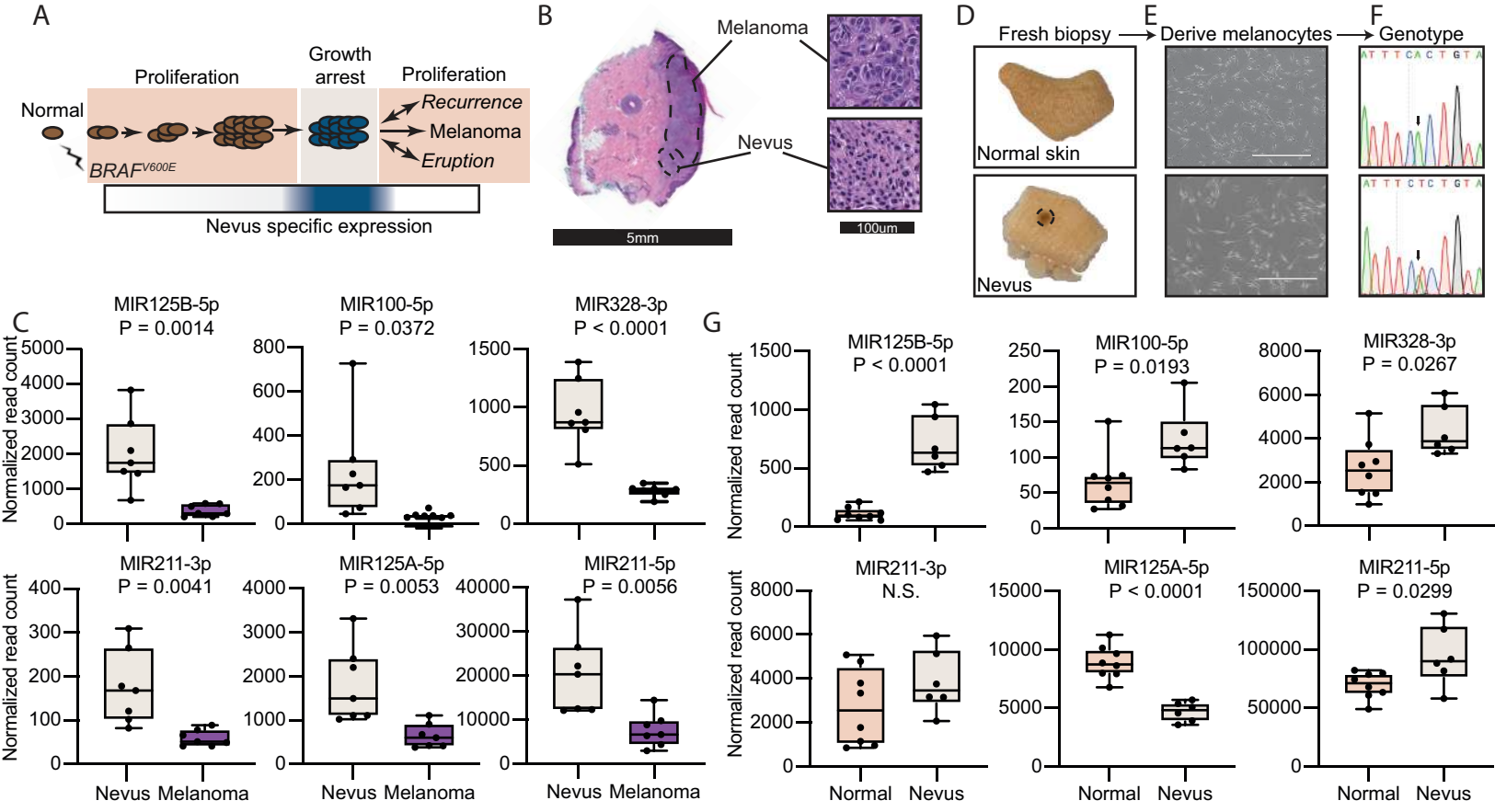
A
Proliferation
Growth arrest
Proliferation
Normal
Recurrence
Melanoma
Eruption
BRAFV600E
Nevus specific expression
B
Melanoma
Nevus
5mm
100um
D
Fresh biopsy
E
Derive melanocytes
F
Genotype
Normal skin
Nevus
C
MIR125B-5p
P = 0.0014
MIR100-5p
P = 0.0372
MIR328-3p
P < 0.0001
MIR211-3p
P = 0.0041
MIR125A-5p
P = 0.0053
MIR211-5p
P = 0.0056
Normalized read count
Nevus Melanoma
G
MIR125B-5p
P < 0.0001
MIR100-5p
P = 0.0193
MIR328-3p
P = 0.0267
MIR211-3p
N.S.
MIR125A-5p
P < 0.0001
MIR211-5p
P = 0.0299
Normalized read count
Normal Nevus

Figure 1

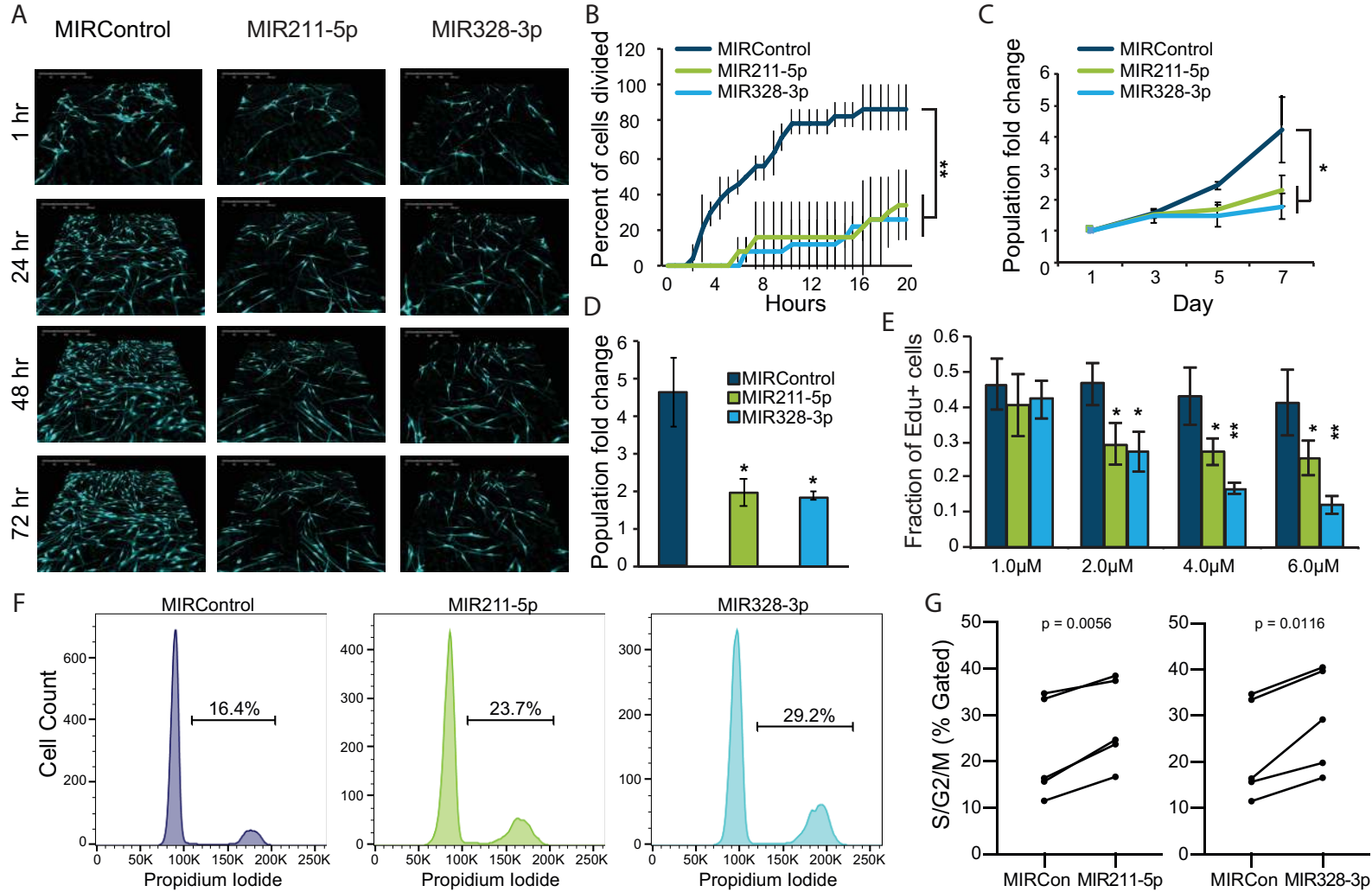
A
MIRControl
MIR211-5p
MIR328-3p
1 hr
24 hr
48 hr
72 hr
B
Percent of cells divided
MIRControl
MIR211-5p
MIR328-3p
Hours
**
C
Population fold change
Day
*
D
Population fold change
*
E
Fraction of Edu+ cells
1.0μM
2.0μM
4.0μM
6.0μM
F
MIRControl
MIR211-5p
MIR328-3p
Cell Count
16.4%
23.7%
29.2%
Propidium Iodide
G
S/G2/M (% Gated)
p = 0.0056
p = 0.0116
MIRCon
MIR211-5p
MIR328-3p

Figure 2

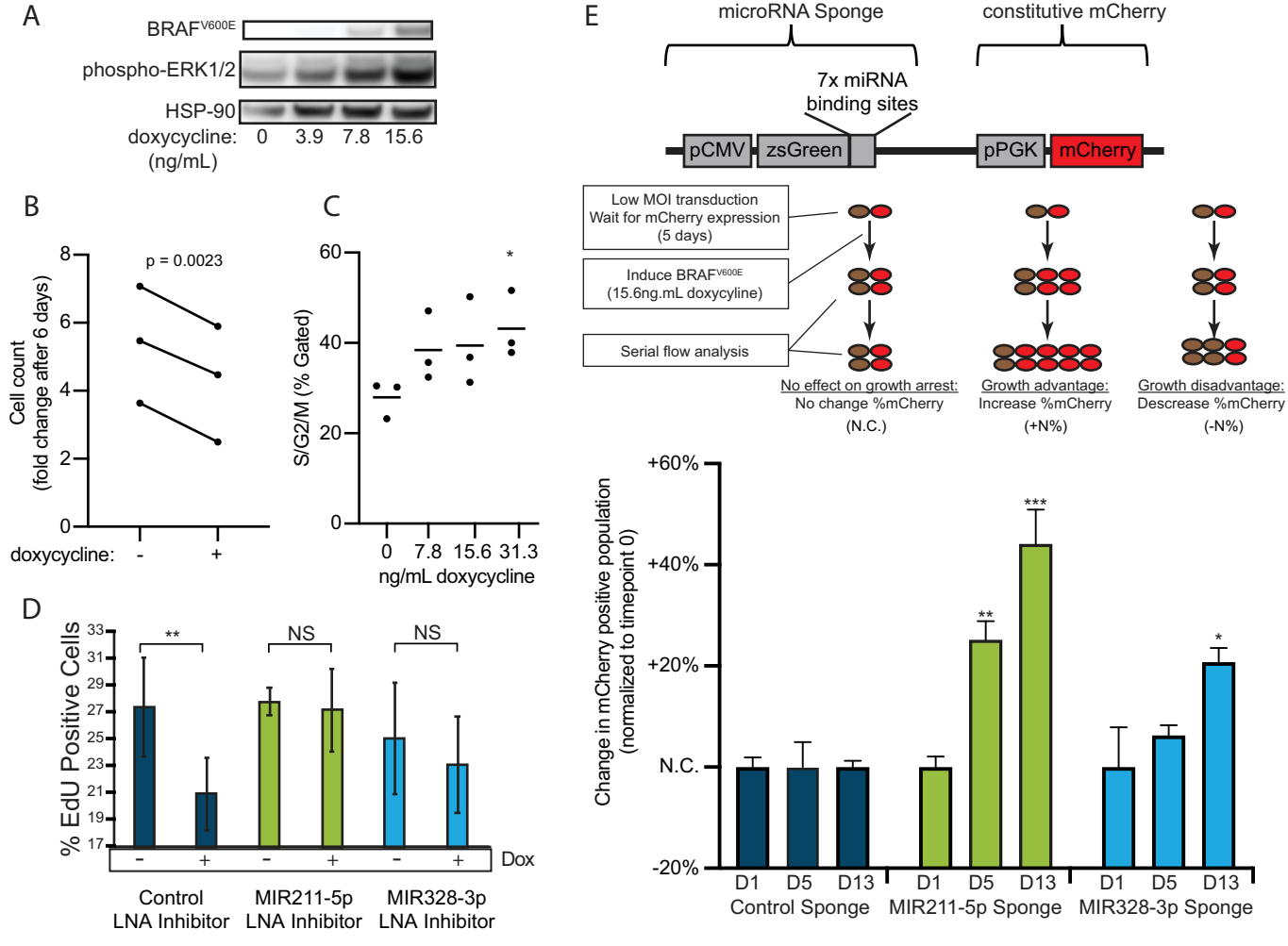
A
BRAFV600E
phospho-ERK1/2
HSP-90
doxycycline: 0 3.9 7.8 15.6
(ng/mL)
B
p = 0.0023
Cell count
(fold change after 6 days)
doxycycline: - +
C
S/G2/M (% Gated)
0 7.8 15.6 31.3
ng/mL doxycycline
D
% EdU Positive Cells
Dox
Control
LNA Inhibitor
MIR211-5p
LNA Inhibitor
MIR328-3p
LNA Inhibitor
E
microRNA Sponge
constitutive mCherry
7x miRNA
binding sites
pCMV
zsGreen
pPGK
mCherry
Low MOI transduction
Wait for mCherry expression
(5 days)
Induce BRAFV600E
(15.6ng.mL doxycyline)
Serial flow analysis
No effect on growth arrest:
No change %mCherry
(N.C.)
Growth advantage:
Increase %mCherry
(+N%)
Growth disadvantage:
Descrease %mCherry
(-N%)
Change in mCherry positive population
(normalized to timepoint 0)
+60%
+40%
+20%
N.C.
-20%
D1 D5 D13
Control Sponge
MIR211-5p Sponge
MIR328-3p Sponge

Figure 3

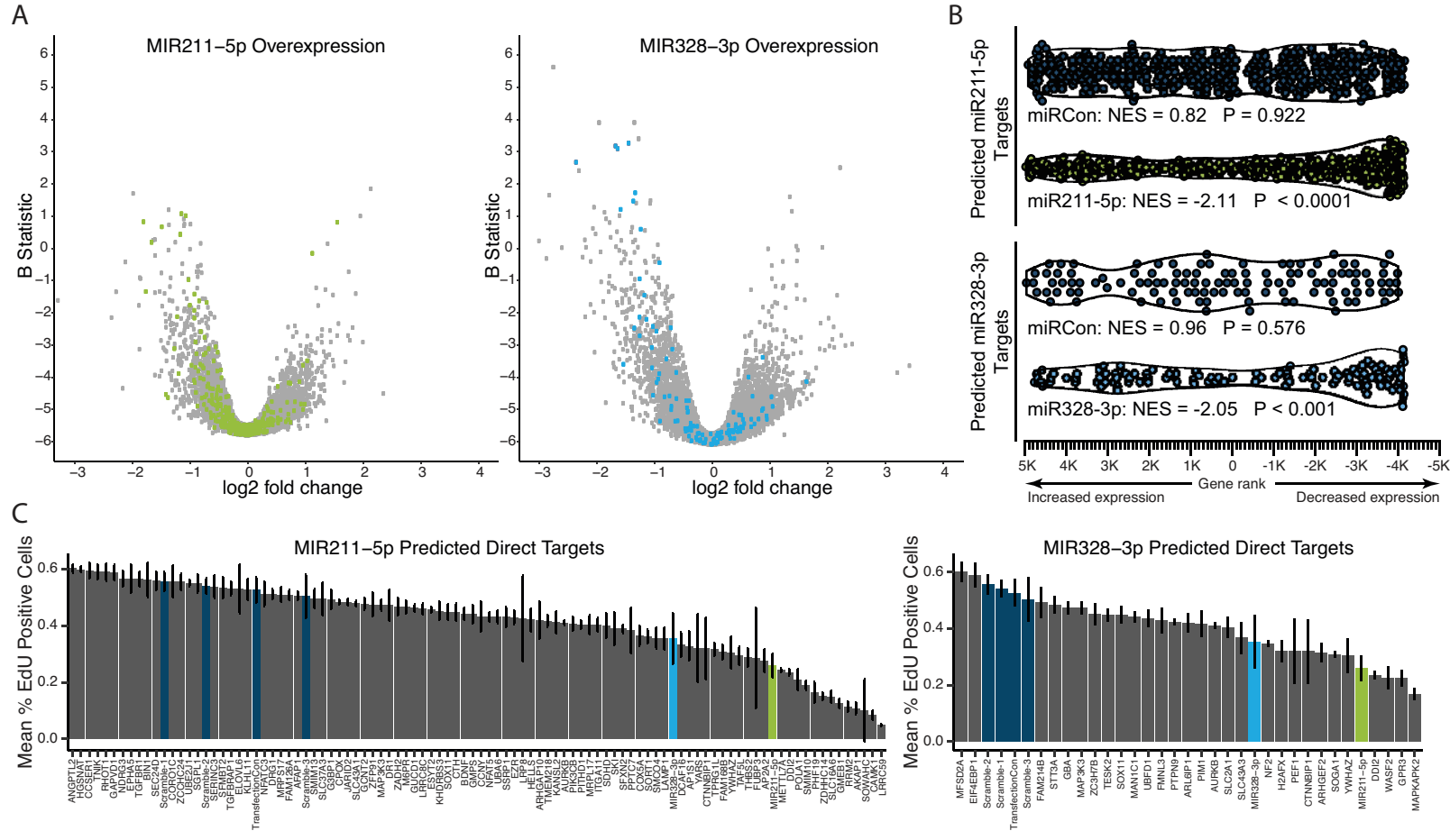
A
MIR211−5p Overexpression
MIR328−3p Overexpression
B Statistic
log2 fold change
B
Predicted miR211-5p Targets
miRCon: NES = 0.82 P = 0.922
miR211-5p: NES = -2.11 P < 0.0001
Predicted miR328-3p Targets
miRCon: NES = 0.96 P = 0.576
miR328-3p: NES = -2.05 P < 0.001
Gene rank
Increased expression
Decreased expression
C
MIR211−5p Predicted Direct Targets
MIR328−3p Predicted Direct Targets
Mean % EdU Positive Cells

Figure 4

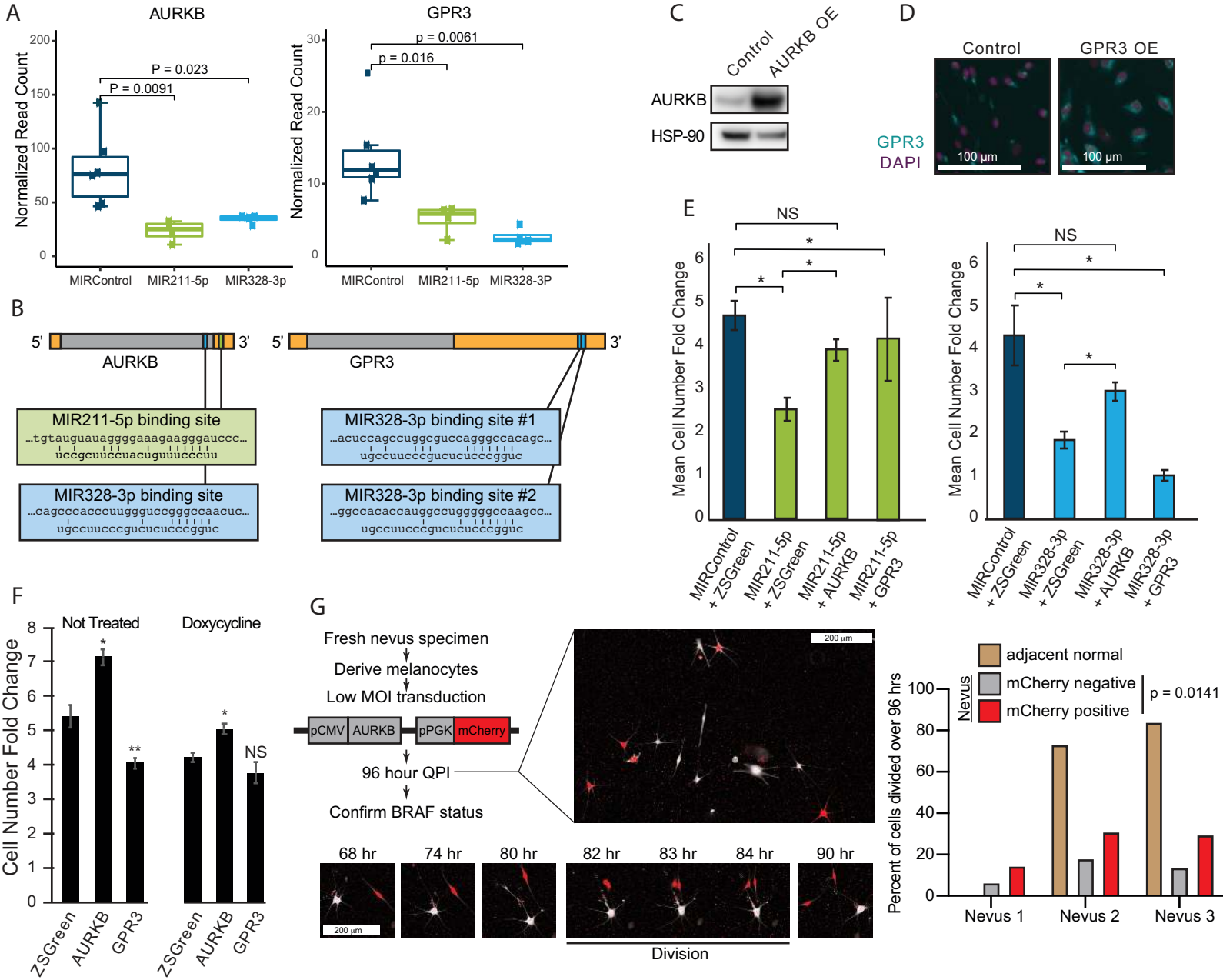
A
AURKB
GPR3
Normalized Read Count
P = 0.023
P = 0.0091
p = 0.0061
p = 0.016
MIRControl
MIR211-5p
MIR328-3p
MIR328-3P
B
5'
3'
AURKB
GPR3
MIR211-5p binding site
MIR328-3p binding site
MIR328-3p binding site #1
MIR328-3p binding site #2
C
Control
AURKB OE
AURKB
HSP-90
D
Control
GPR3 OE
GPR3
DAPI
100 µm
E
Mean Cell Number Fold Change
NS
MIRControl + ZSGreen
MIR211-5p + ZSGreen
MIR211-5p + AURKB
MIR211-5p + GPR3
MIR328-3p + ZSGreen
MIR328-3p + AURKB
MIR328-3p + GPR3
F
Not Treated
Doxycycline
Cell Number Fold Change
ZSGreen
AURKB
GPR3
NS
G
Fresh nevus specimen
Derive melanocytes
Low MOI transduction
pCMV
AURKB
pPGK
mCherry
96 hour QPI
Confirm BRAF status
200 µm
68 hr
74 hr
80 hr
82 hr
83 hr
84 hr
90 hr
Division
adjacent normal
Nevus
mCherry negative
mCherry positive
p = 0.0141
Percent of cells divided over 96 hrs
Nevus 1
Nevus 2
Nevus 3

Figure 5

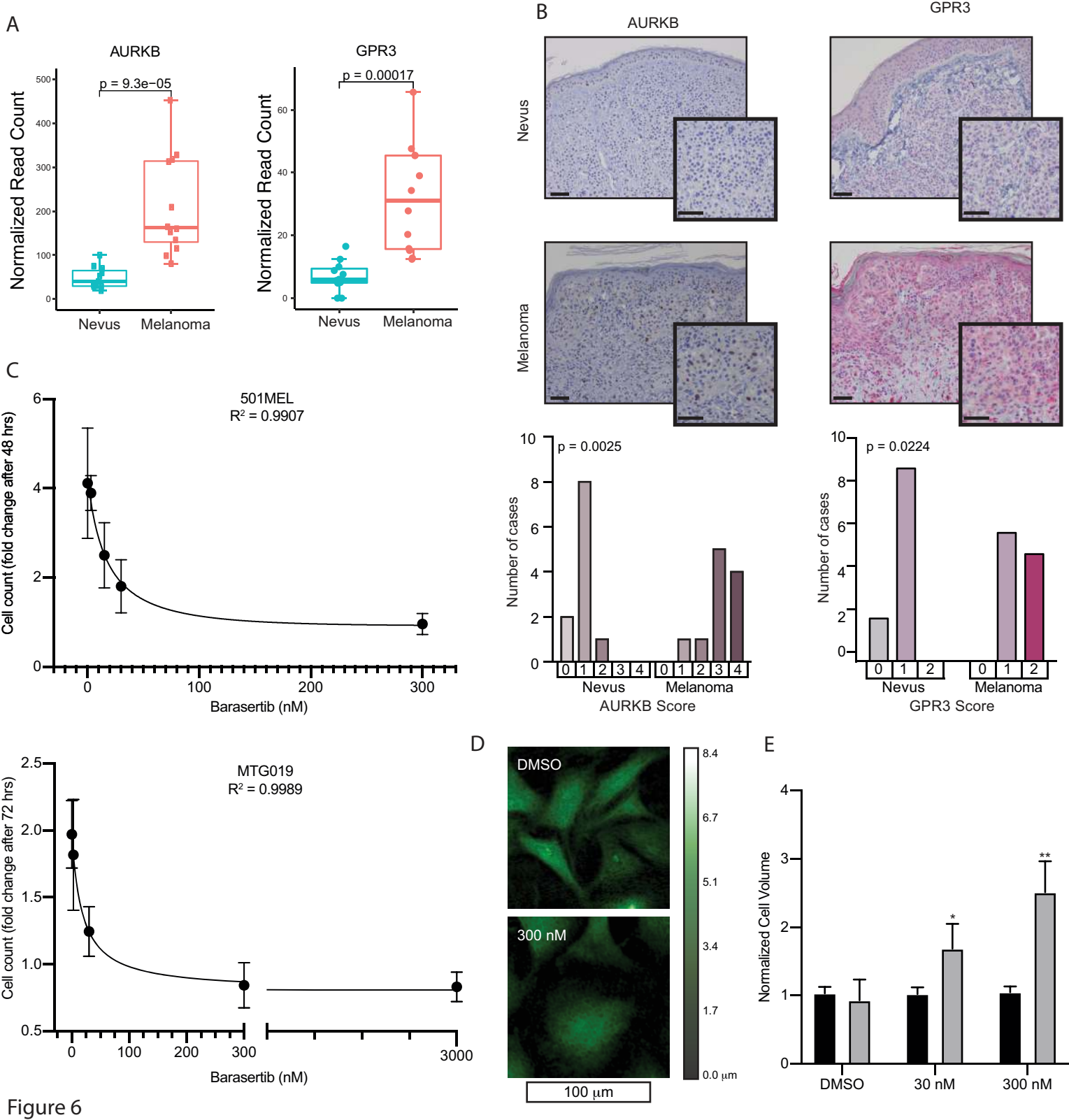
A
AURKB
GPR3
p = 9.3e−05
p = 0.00017
Normalized Read Count
Nevus
Melanoma
B
AURKB
GPR3
Nevus
Melanoma
p = 0.0025
p = 0.0224
Number of cases
AURKB Score
GPR3 Score
C
501MEL
R² = 0.9907
Cell count (fold change after 48 hrs)
Barasertib (nM)
MTG019
R² = 0.9989
Cell count (fold change after 72 hrs)
Barasertib (nM)
D
DMSO
300 nM
100 µm
E
Normalized Cell Volume
DMSO
30 nM
300 nM

Figure 6

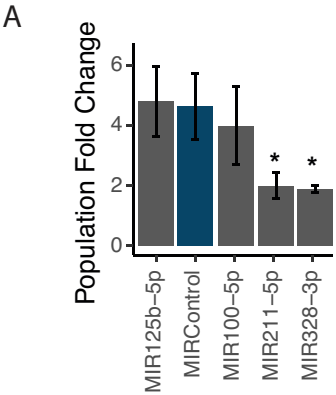
A
Population Fold Change
0
2
4
6
*
*
MIR125b–5p
MIRControl
MIR100–5p
MIR211–5p
MIR328–3p

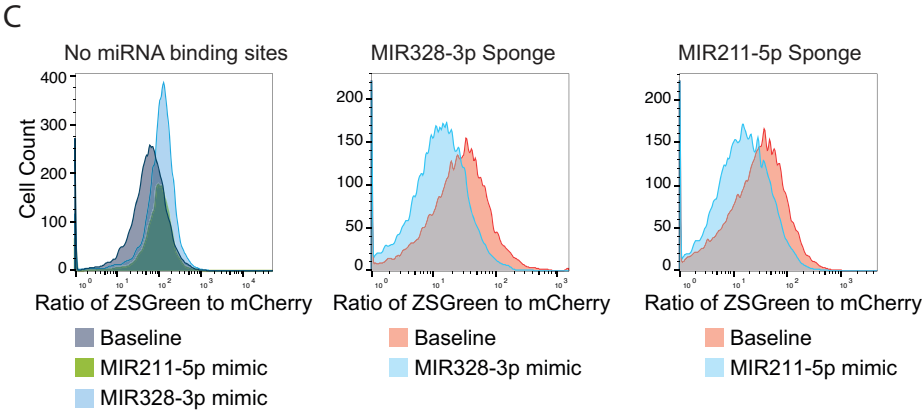
C
No miRNA binding sites
MIR328-3p Sponge
MIR211-5p Sponge
Cell Count
Ratio of ZSGreen to mCherry
Baseline
MIR211-5p mimic
MIR328-3p mimic
Baseline
MIR328-3p mimic
Baseline
MIR211-5p mimic

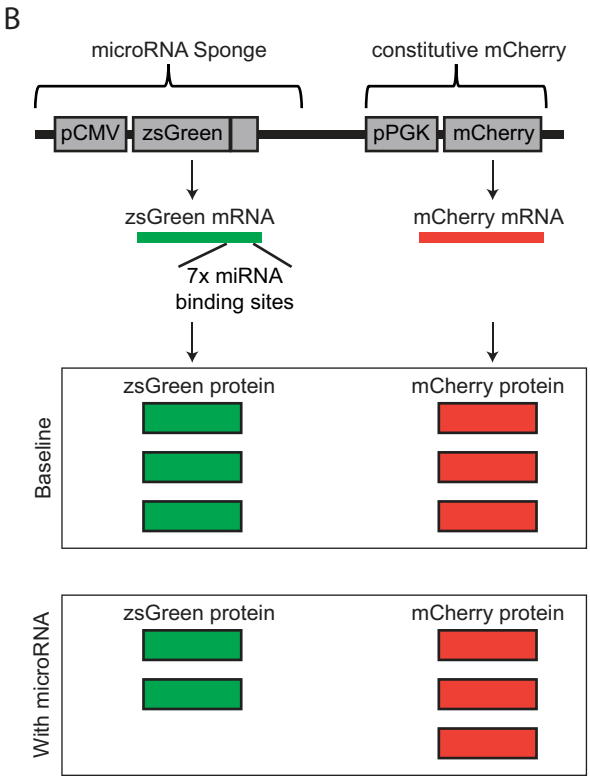
B
microRNA Sponge
constitutive mCherry
pCMV
zsGreen
pPGK
mCherry
zsGreen mRNA
mCherry mRNA
7x miRNA
binding sites
zsGreen protein
mCherry protein
Baseline
zsGreen protein
mCherry protein
With microRNA

Figure S1

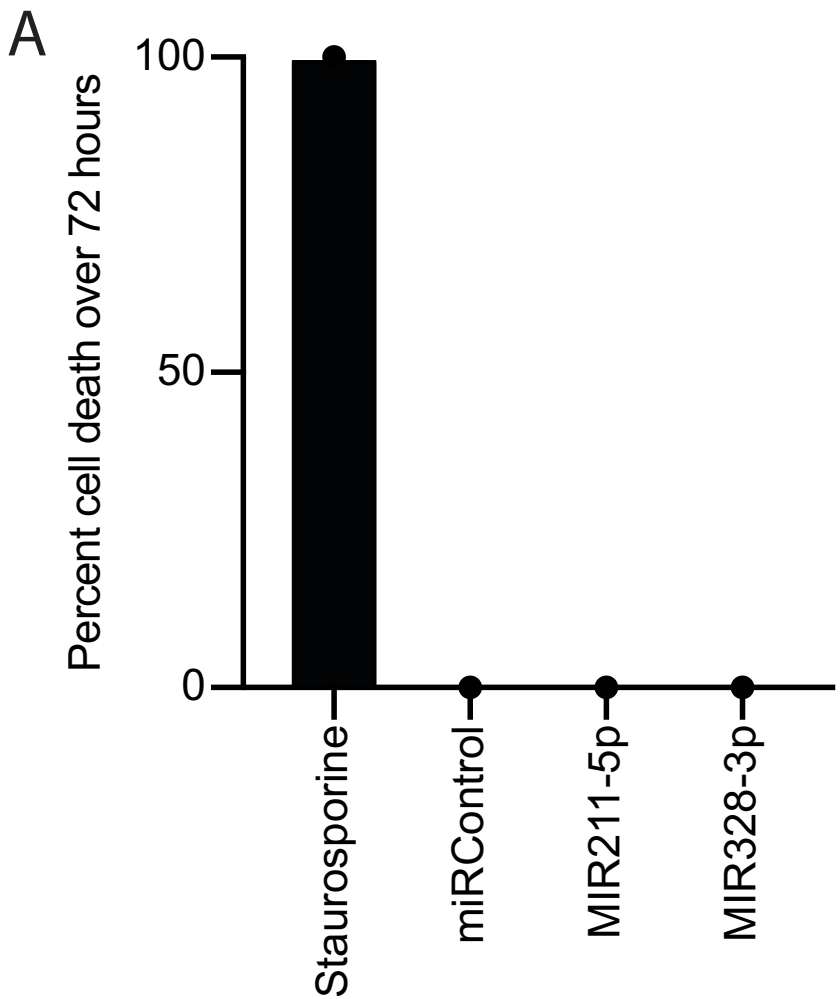
A
Percent cell death over 72 hours
100
50
0
Staurosporine
miRControl
MIR211-5p
MIR328-3p

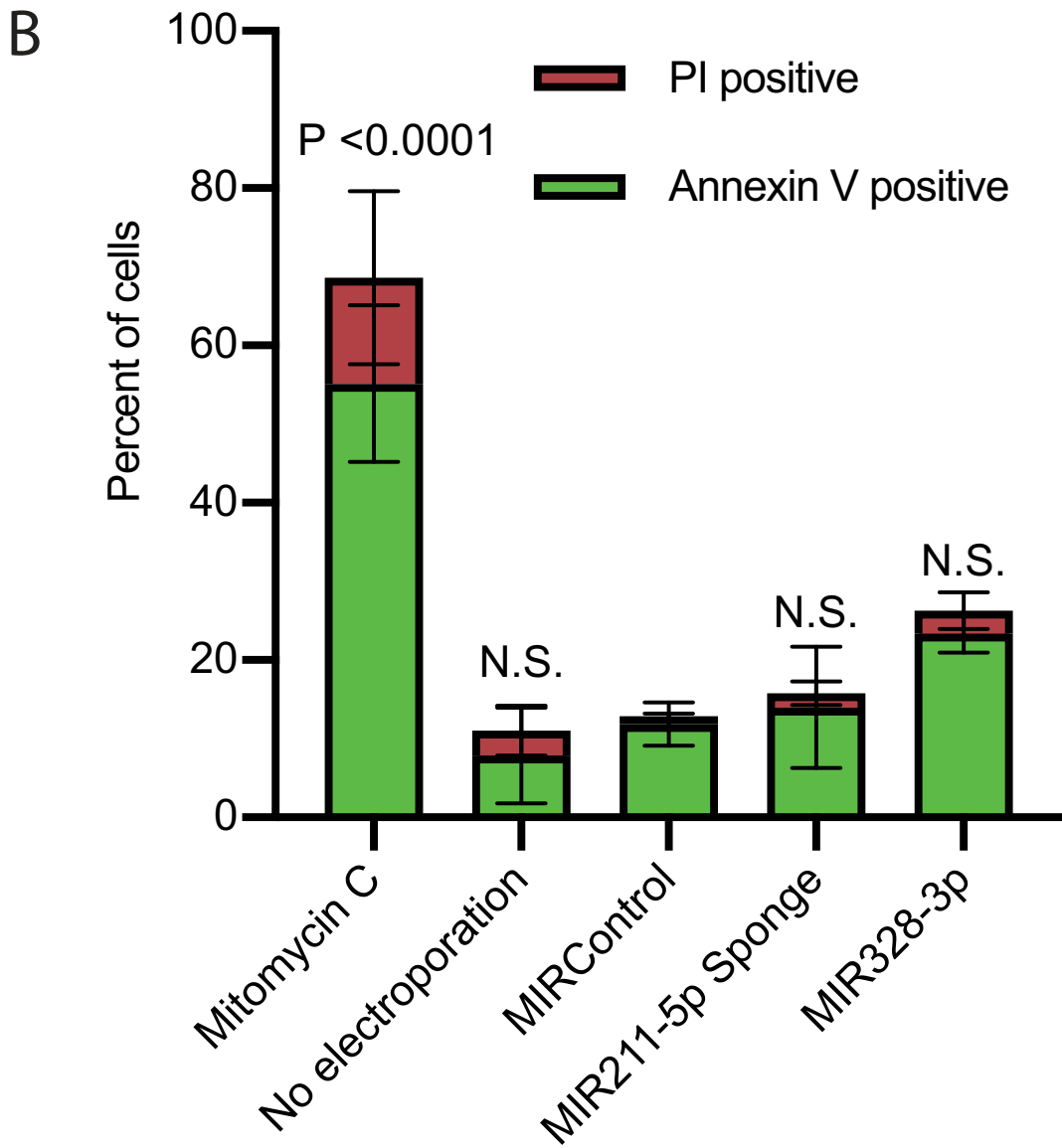
B
Percent of cells
100
80
60
40
20
0
PI positive
Annexin V positive
P <0.0001
N.S.
N.S.
N.S.
Mitomycin C
No electroporation
MIRControl
MIR211-5p Sponge
MIR328-3p

Figure S2